

Mechanical Characteristics of a Roll-Bonded Cu-Clad Steel Sheet Processed Through Incremental Forming



HONGYU WEI and G. HUSSAIN

Incremental sheet forming (ISF) is an emerging cold forming process with a high economic payoff. In this study, the influence of the ISF process on the tensile properties of Cu-clad Steel sheet is analyzed experimentally. Depending on the forming conditions, the post-ISF values of yield strength, tensile strength, and ductility are found to range from 161 to 430, 288 to 449 MPa, and 4.93 to 16.62 pct, respectively. These properties show a strong dependence on several correlated quantities such as the applied plastic strain, grain size, and mean residual stress. As the plastic strain increases from 0.08 to 0.8, the width of the grain decreases from 8.11 to 5.78 μm and the residual stress increases from -15 to -131 MPa. In comparison to the unformed sheet, ISF enhances the yield strength (4.6 to 117 pct) and tensile strength (0.6 to 73 pct). The nature of change in ductility (-67 to 117 pct), however, depends on the process conditions, especially the state of the unformed sheet (*i.e.*, rolled/annealed) and the value of applied strain. In general, the rolled (or prestrained) sheet upon ISF experiences an increase in ductility. The annealed sheet, however, sees a drop in ductility when the forming strains are low (*e.g.*, < 0.4) and an increase in ductility when the strains are high (*e.g.*, > 0.4). X-ray diffraction (XRD) and electron dispersive spectroscopy (EDS) analyses confirm that no new phase formed during ISF.

<https://doi.org/10.1007/s11661-019-05366-y>

© The Minerals, Metals & Materials Society and ASM International 2019

I. INTRODUCTION

THE tensile properties of a material are extensively used as the basic input(s) in the design and manufacturing of components. For instance, the yield strength is employed as a criterion parameter for designing structural components (*e.g.*, gas containers). This also determines the onset of yielding to produce parts through plastic deformation. The tensile strength defines the onset of instability if there is necking or the occurrence of fracture, and it is also used as a base property to determine the forming force in metal forming processes such as deep drawing and bending. The percent elongation (or ductility) and hardening exponent are alternatively used to indicate the formability in several forming processes, *e.g.*, stamping, hydroforming, and incremental forming.^[1-3]

A wide range of shaping processes make use of deformation to manufacture components. This type of processing substantially affects the mechanical properties and microstructure of the components produced. Serajzadeh and Mohammadzadeh^[4] studied the effect of rolling reduction, rolling speed, and temperature on the yield strength of low-carbon steel. They observed an increase in yield strength with increasing rolling reduction and speed, attributing this to grain refinement and increased dislocation density. The yield strength, on the contrary, decreased with increasing forming temperature due to a reduction in dislocation density. Zhao *et al.*^[5] investigated the role of extrusion-wheel velocity on various mechanical properties and found that the tensile strength and hardness of AA6061 both increased with increasing wheel velocity; however, excessive velocity caused a slight reduction in these properties. They attributed these findings to the combined effect of reduction in grain size and process-induced heating.

Balogun *et al.*^[6] analyzed the influence of deformation on the mechanical properties of AA6063 alloy during cold rolling and forging processes. According to the results, the tensile strength and hardness increased while the ductility decreased as the percent reduction increased. Mo *et al.*^[7] analyzed the effect of loading orientation (*i.e.*, 0 to 90 deg) on the tensile strength of columnar-grained HA117-2 aluminum bronze. They

HONGYU WEI is with the College of Mechanical & Electrical Engineering, Nanjing University of Aeronautics & Astronautics, Nanjing, 210016, P.R. China. G. HUSSAIN is with the Faculty of Mechanical Engineering, GIK Institute of Engineering Sciences & Technology, Topi, 23640, Pakistan. Contact email: gh_ghumman@hotmail.com

Manuscript submitted November 5, 2017.

Article published online July 22, 2019

observed that the material achieved greater strength with orientations of 45 and 60 deg. Sepahi-Boroujeni and Sepahi-Boroujeni^[8] observed mechanical improvements in the H-Tube pressing (HTP) of AZ-80 magnesium alloy. Applying half-cycle HTP, they recorded a 90 pct gain in yield strength and a 100 pct gain in tensile strength due to grain refinement. Figueiredo and Langdon^[10] observed similar results when the AZ31 magnesium alloy was processed by equal channel angular pressing. Xu *et al.*^[9] found that the processing of AZ31 alloy through high-pressure torsion increased the microhardness and reduced the grain size. These variations further affect the residual stresses in the formed material.^[11]

Incremental sheet forming (ISF) is a novel forming process that performs dieless forming on the metallic and nonmetallic sheets. In this process, a general purpose spherical-end tool systematically follows a predefined trajectory to produce sculptured shapes. This manner of shaping renders ISF a promising and cost-effective alternative to traditional pressing and spinning processes. However, being slow, it is economically suitable only for short production runs. The process has found numerous applications in various sectors such as in the biomedical and automobile areas.^[12]

The forming conditions affect the deformation in the ISF process. For instance, the size of the forming tool influences a number of deformation attributes such as the deformation zone, hydrostatic stress, damage, and forming force.^[13–15] The step size controls the damage and forming force,^[12,15] while the deformation angle defines the sheet thinning, forming force, and material hardening.^[12,16] The feed rate decides the strain rate and strain hardening,^[15] while the tool rotation controls the friction and microstructure.^[17] The hydrostatic stress, damage, strain hardening, and microstructure are among the important factors that determine the mechanical performance of the formed material.^[1] Therefore, a material upon ISF can experience significant changes in mechanical properties.

In this regard, Jeswiet *et al.*^[18] performed ISF on aluminum sheet over a range of deformation angles and subjected the formed sheet to tension tests. They found that the sheet experienced an increase in strength at the cost of ductility. This result was a good addition to the knowledge base, although the role of other parameters (*e.g.*, step size, feed rate, tool diameter, tool rotation, and material condition) is missing and needs to be investigated. Ulacia *et al.*^[19] observed a twinned structure when analyzing the effect of warm ISF on the Mg alloy. Comparing the effects of ISF and uniaxial stretching, they further concluded that the ISF process generated more twins. Recently, Lozano-Sánchez *et al.*^[20] studied the effect of ISF on the mechanical performance of polypropylene-MWCNT composite sheet. The tension tests revealed that the composite achieved a gain in both strength and ductility and explained this by the fact that the forming tool aligned the molecular chains during forming.

Nowadays, applications of clad sheet metals, also regarded as layered sheet metals, are increasing as these offer a superior combination of properties compared to their constituents. These metals are produced by joining multiple monolithic sheets. The resulting layered sheet owing to a mix of properties demonstrates complex deformation behavior,^[21] as a result. Therefore, the knowledge generated for the forming of monolithic sheet metals may not be directly applicable to the clad sheet metals.

From the preceding literature review, it can be identified that, first, the list of parameters affecting the post-ISF tensile properties of sheet metals is not complete and, second, such an investigation with a focus on the clad sheet metal(s) is missing. Moreover, any change in the properties due to deformation is associated with variations in the microstructure and residual stresses. Therefore, the present study is aimed at investigating the post-ISF tensile properties of a clad sheet metal from the perspective of process parameters, microstructure, and residual stresses.

In view of its potential applications in the automobile and nuclear industries (*e.g.*, radiator and reactor), roll-bonded Cu-clad Steel sheet is employed as the experimental material. The sheet is shaped into a series of pyramids by varying six process parameters. Tensile samples are cut from the pyramids and stretched to fracture to determine tensile properties, namely, yield strength, tensile strength, and ductility. The effects of various process parameters are analyzed and quantified by making use of the statistical response surface methodology approach. Hole drill tests are conducted to reveal a relationship between the properties and residual stress in the formed sheet. Microscopy, electron dispersive spectroscopy (EDS), and X-ray diffraction (XRD) examinations are performed to examine microstructure changes in the formed sheet, if any, and their corresponding effects on tensile properties. From these analyses, useful knowledge is generated that establishes an in-depth understanding of the property-parameter and property-deformation-microstructure-stress correlations in ISF.

II. EXPERIMENTAL PROCEDURES

The design of experiment (DoE) approach was employed to analyze the post-ISF tensile properties of the Cu/Steel clad sheet in this study. The response surface, Taguchi, and full factorial designs are three main designs that are in regular practice for conducting the DoE. The Taguchi design requires the least number of tests, but it does not adequately analyze the interactive effects. The full factorial design, on the other hand, has the benefit of analyzing the combined effects. However, it requires a greater number of experiments. The response surface design demands experiments somewhere in between the other two DoE approaches without compromising the accuracy of the analysis.^[22]

Therefore, a standard D-optimal response surface design of the following form was applied:

$$Y = f(X_1, X_2, X_3 \dots X_n) + E \quad [1]$$

where X_i is the process parameter, E is the error due to noise, and Y is the response surface.

The process parameters along with the respective limits (low/high) employed for the present study are shown in Table I, while the relevance of these parameters with the aim of this study was elaborated in Section I. Special attention was paid on achieving a high deformation angle θ in ISF while selecting the limits of parameters, as the angle is a direct measure of applied strain and strain hardening.^[18] The target high limit of the angle was set to 60 deg, and the low limit was 20 deg because further decreases in the angle led to formation of defects (*e.g.*, pillow). The low limit of the tool diameter d was selected as 6 mm, for very small tools (when $d \leq 5t_o$, where t_o is the sheet thickness) severely shear the material, causing premature sheet failure.^[14] The high limit of the tool diameter was set to 20 mm, as the target angle of 60 deg could not be achieved when the diameter was further increased. A similar reason was considered for selecting the high limit of the step size p (*i.e.*, 1 mm). The low limit of the step size (*i.e.*, 0.2 mm), however, was set keeping in view the fact that the production time increases with decreases in step size. The limits of the feed rate f (1000 to 3500 mm/min) and the spindle rotation ω (500 to 3000 rpm) were chosen considering both the production time and machine specifications. The high limit of the annealing temperature T was set to 700 °C since further increases in temperature resulted in detachment of the laminates. The state of as-received Cu/Steel sheet (*i.e.*, rolled and nonannealed) was regarded as the low limit of temperature and was designated as 0 °C.

Nowadays, statistical packages are available to design the experimental plans. The authors used the Design Expert DX-10 package. The parameters with the respective levels listed in Table I were fed into this package, which turned out a plan of 38 runs. As presented in Table II, the plan varies each parameter over five levels and contains four replicates in order to account for repeatability. The statistical design evaluation process proposed a second-order polynomial as a suitable model to fit the experimental data, because higher order models resulted in aliased terms (*i.e.*, 3-factor interactions). The suitability of the second-order polynomial was validated, ensuring the minimum degree

of freedom (DoF) to be 3 for “lack of fit” and 4 for “pure error.” As the design satisfied the minimum criteria of DoF, the test plan was deemed to be robust, having sufficient design points and replicates. Because of their importance in component design, as explained in Section I, the tensile properties were measured as the main outcomes (or responses) of the DoE. The particular properties include the yield strength σ_y , tensile strength σ_t , and elongation pct λ .

In order to execute the plan, a frustum of the pyramid was employed as the test geometry. The dimensions of the pyramid are shown in Figure 1(a). The Cu-clad Steel sheet was employed as the experimental material (Figure 1(b)). The sheet was fabricated by rolling the DCO4 Steel (99.75 pct Fe) and the H90 Cu (91 pct Cu) laminates stacked in the order of Cu/Steel/Cu. The bonding was realized at 50 pct reduction, resulting in the final thickness of 1 mm, where the Steel laminate was 0.9-mm thick and each of the Cu laminates was 0.05-mm thick. The rolled sheet was then annealed over a range of temperatures (0 °C to 700 °C, where 0 refers to the nonannealed or as-received condition), as listed in Table II. For this purpose, the material was held in the carbolite induction furnace for 2 hours. The sheet was cut into 80 mm × 180 mm × 1 mm blanks, which were then clamped in the fixture and subjected to forming with HSS spherical-end tools. The motion of the forming tool while forming was controlled by a CNC milling machine. In this study, a range of forming tools were manufactured and used in accordance with the experimental plan.

The ISF process, depending on the conditions, induces plastic strain in the sheet. This strain was determined by applying the following relation:

$$\varepsilon_{\text{-ISF}} = |\ln(t/t_o)| \quad [2]$$

where $\varepsilon_{\text{-ISF}}$ is the applied plastic strain, t_o is the thickness of the sheet prior to forming, and t is the thickness of the sheet after forming. The thickness t was measured with a Vernier caliper at an accuracy of ± 0.01 mm.

The sheet during ISF was reported to experience plane-strain stretching (*e.g.*, on the flats of the pyramid) and biaxial stretching (*e.g.*, on the corners of the pyramid).^[13] Since plane-strain stretching is the dominant deformation mode in ISF, the effect of ISF processing on the tensile properties was quantified only for this mode. Tensile samples following the ASTM E8 standard were prepared from the flat sides of the formed pyramids, and the long axis of the tensile sample was maintained along the stretching direction (*i.e.*, 2, as shown in Figure 1(c)). The test samples were stretched to fracture (Figure 1(d)) on an Instron universal testing machine, where the crosshead speed was maintained at 2 mm/min.

Microscopic examinations were performed on samples that were fine polished and etched with Keller’s reagent. The polished surfaces were observed with an optical microscope and a scanning electron microscope (SEM) (CMM-22E and Philips XL 30, respectively). XRD and EDS analyses were performed to detect any

Table I. Parameters and Respective Levels Employed in the Current Study

| Parameter | Symbol | Unit | Low | High |
|-----------------------|----------|--------|------|------|
| Tool Diameter | d | mm | 6 | 20 |
| Deformation Angle | θ | deg | 20 | 60 |
| Rotation | ω | rpm | 500 | 3000 |
| Feed Rate | f | mm/min | 1000 | 3500 |
| Step Size | p | mm | 0.2 | 1 |
| Annealing Temperature | T | °C | 0 | 700 |

new phase if it developed due to ISF processing. The XRD analysis was performed at a scanning speed of 6 deg/min using a Rigaku Y-Q4 apparatus, while the EDS analysis was conducted with an analyzer made by Oxford Instruments Company.

The residual stresses were determined by conducting the hole drill tests in accordance with the ASTM E837-13a standard. To do so, a sample piece was cut from each of the pyramids using an EDM wire cut machine. The strain rosette (HT Sensor) was attached to the surface, as indicated in Figure 1(e), with the epoxy. The drilling operation was performed on the surface using a Juhang JH-30 drilling rig and a drill bit having a diameter of 0.8 mm. The in-plane principal strains (ϵ_1 and ϵ_2) were recorded on a P3 strain indicator and were later transformed into the corresponding in-plane stresses (σ_1 and σ_2). The profiles of these stresses revealed that the stress value gradually declined from the surface to the subsurface level. Therefore, a mean value of a principal stress (*i.e.*, σ_m) was obtained and used in the analysis.

III. RESULTS AND DISCUSSION

A. Significant Parameters

One of the objectives of the current study was to identify the significant parameters affecting tensile properties. For this purpose, an analysis of variance (ANOVA) was conducted on the measured responses (*i.e.*, tensile properties listed in Table II). *F*-value and *P*-value are two of the important outputs of ANOVA upon which the significance of a term is decided.^[22] The *F*-value compares the source mean square to the residual mean square, and the *P*-value is the probability of getting an observed *F*-value if the term did not have any effect on the response. The *P*-value, in simple words, indicates the influence of noise (any external source) on the occurrence of an *F*-value. Therefore, the smaller its *P*-value, the more significant a term will be. In general, a term that has a *P*-value of ≤ 0.05 would be considered a significant effect. The *F*- and *P*-values for the terms of three considered responses are presented in Table III wherein the significant terms are indicated with “Y.” From Table III, it can be observed that there are 28 sources of variations out of which 27 originated from the parameters (*i.e.*, standalone parameters, cross-interactions, and self-interactions) and one initiated from the quadratic fit model. A cross-interaction (*e.g.*, *dp*) dictates that the nature of the effect of a parameter on a response is associated with the value of the interactant. The most and least significant cross-interactions, respectively, include θT and fT for the yield strength (σ_y), *dp* and fT for the tensile strength (σ_t), and θT and df for the ductility or elongation (λ). The correlation(s) between the tensile properties and various parameters is discussed in Section III-B.

B. Correlation Between Tensile Properties and Technological Parameters

Table II shows that the post-ISF tensile properties obtained from 38 tests depend on the technological parameters. The significance of these parameters was

discussed earlier and their effects on the tensile properties are presented in Figures 2 through 4. The properties plotted in these graphs represent the process effects in the plane-strain mode, detailed as follows.

Figures 2(a) through (e) depict the relationship between various parameters and the post-ISF yield strength σ_y of the Cu/Steel clad sheet. The yield strength, irrespective of the interacting parameters, steadily decreases as the annealing temperature *T* increases from 0 °C to 700 °C (Figures 2(a), (d), and (e)). The yield strength, on the contrary, increases with an increase in the deformation angle θ . A similar trend can be observed with increasing the tool diameter *d* when the step size *p* is large (1 mm) (Figure 2(b)). However, there is a slight decrease in the yield strength with increasing tool diameter when the step size is low (0.2 mm). For the nonannealed/rolled clad sheet (0 °C), the yield strength increases as the tool diameter increases (Figure 2(a)). On the other hand, for the sheet annealed at 700 °C, the yield strength slightly decreases as the tool diameter increases from 6 to 20 mm.

The nature of the effects of step size *p*, rotation ω , and feed rate *f* are similar (Figures 2(b), (d), and (e)). The yield strength initially increases with an increase in either of these parameters. However, after a certain value, the same drops as the value of either of these parameters increases (*e.g.*, 0.6 mm for the step size, 1750 rpm for the rotation, and 2250 mm/min for the feed rate).

The post-ISF tensile strength of the Cu/Steel clad sheet is shown in Figures 3(a) through (d). Comparing Figure 3 with Figure 2, it is observable that the effects of the parameters on the tensile strength, in most respects, are similar to those observed for the yield strength. However, certain discrepancies can be noticed as well. For example, the effect of the feed rate on the yield strength is independent of the annealing temperature (Figure 2(e)), while its effect on tensile strength shows a dependence on the annealing temperature. When the annealing temperature is high (700 °C), the tensile strength steadily increases with the feed rate over the entire range (Figure 3(c)). However, when the temperature is low (0 °C), the tensile strength instead diminishes with the increasing feed rate. Thus, regardless of the feed rate, the post-ISF tensile strength remains higher than that of the starting blank.

Figures 4(a) through (c) present the influence of parameters on the post-ISF ductility of the clad sheet. The ductility, contrary to the yield strength and tensile strength, decreases with the increasing tool diameter when the step size is high (1 mm), while the same decreases when the step size is low (0.2 mm) (Figure 4(a)). Similar effects can be observed pertaining to the tool diameter and feed rate (Figure 4(b)). As observed in Figure 4(c), the nature of the effect of the deformation angle is associated with the annealing temperature. The ductility substantially decreases with the increasing deformation angle when the temperature is high (*e.g.*, 700 °C), while it slightly increases when the temperature is low (*e.g.*, 0 °C). The post-ISF ductility increases sharply as the annealing temperature increases when the clad sheet is deformed to a low angle (*e.g.*,

Table II. Experimental Plan and Results

| Test | d (mm) | θ (Deg) | ω (rpm) | f (mm/min) | T (°C) | p (mm) | σ_y (MPa) | σ_t (MPa) | λ (Pct) | Pct σ_y | Pct σ_t | Pct λ |
|------|----------|----------------|----------------|--------------|----------|----------|------------------|------------------|-----------------|----------------|----------------|---------------|
| 1 | 6 | 60 | 500 | 1000 | 0 | 0.2 | 426 | 445.7 | 5.67 | 140.68 | 54.33 | 53.24 |
| 2 | 20 | 20 | 1750 | 3500 | 700 | 0.2 | 168 | 295.4 | 16.32 | 46.09 | 15.84 | 8.8 |
| 3 | 6 | 20 | 3000 | 3500 | 0 | 0.2 | 198 | 294.6 | 6.35 | 11.86 | 2.01 | 71.62 |
| 4 | 20 | 60 | 3000 | 1000 | 350 | 0.2 | 410 | 436.5 | 5.48 | 182.76 | 57.58 | 21.78 |
| 5 | 6 | 46.7 | 500 | 2666 | 0 | 1 | 363 | 402.7 | 7.47 | 105.08 | 39.44 | 101.89 |
| 6 | 20 | 20 | 500 | 3500 | 0 | 1 | 202 | 290.4 | 7.03 | 14.12 | 0.55 | 90 |
| 7 | 20 | 20 | 3000 | 1000 | 700 | 0.47 | 164 | 296.3 | 15.94 | 42.61 | 16.19 | 6.27 |
| 8 | 20 | 20 | 3000 | 3500 | 466 | 1 | 177 | 298.6 | 9.87 | 36.15 | 10.18 | 73.16 |
| 9 | 13 | 20 | 3000 | 1000 | 0 | 0.2 | 194 | 292.4 | 5.93 | 9.6 | 1.25 | 60.27 |
| 10 | 15.3 | 60 | 500 | 1000 | 0 | 1 | 427 | 445.6 | 6.04 | 141.24 | 54.29 | 63.24 |
| 11 | 15.3 | 60 | 500 | 1000 | 0 | 1 | 425 | 444.7 | 5.83 | 140.11 | 53.98 | 57.57 |
| 12 | 10.7 | 60 | 500 | 3500 | 233 | 0.2 | 416 | 439.8 | 5.93 | 168.39 | 57.07 | 48.25 |
| 13 | 10.7 | 46.7 | 3000 | 3500 | 0 | 1 | 365 | 408.7 | 7.68 | 106.21 | 41.52 | 107.57 |
| 14 | 6 | 60 | 3000 | 3500 | 700 | 0.2 | 409 | 435.6 | 6.34 | 255.65 | 70.82 | - 57.73 |
| 15 | 15.3 | 60 | 500 | 3500 | 700 | 1 | 407 | 441.3 | 5.38 | 253.91 | 73.06 | - 64.13 |
| 16 | 13 | 40 | 1750 | 2250 | 350 | 0.6 | 353 | 398.2 | 6.93 | 143.45 | 43.75 | 54 |
| 17 | 20 | 60 | 500 | 1000 | 700 | 0.2 | 406 | 430.8 | 5.87 | 253.04 | 68.94 | - 60.87 |
| 18 | 20 | 20 | 500 | 1000 | 0 | 0.2 | 199 | 300.4 | 6.84 | 12.43 | 4.02 | 84.86 |
| 19 | 20 | 60 | 1333 | 3500 | 0 | 1 | 430 | 449.2 | 5.32 | 142.94 | 55.54 | 43.79 |
| 20 | 20 | 20 | 500 | 1000 | 700 | 1 | 166 | 293.5 | 15.69 | 44.35 | 15.10 | 4.6 |
| 21 | 20 | 60 | 3000 | 1000 | 700 | 1 | 409 | 433.2 | 5.67 | 255.65 | 69.88 | - 62.2 |
| 22 | 20 | 60 | 500 | 1000 | 700 | 0.2 | 404 | 429.6 | 4.93 | 251.3 | 68.47 | - 67.13 |
| 23 | 6 | 60 | 3000 | 1833 | 700 | 1 | 407 | 428.3 | 6.26 | 253.91 | 67.96 | - 58.27 |
| 24 | 13 | 40 | 1750 | 2250 | 350 | 0.6 | 356 | 402.7 | 5.98 | 145.52 | 45.38 | 32.89 |
| 25 | 6 | 20 | 500 | 2666 | 0 | 0.2 | 198 | 294.3 | 6.39 | 11.86 | 1.90 | 72.70 |
| 26 | 20 | 46.7 | 500 | 3500 | 0 | 0.2 | 367 | 406.2 | 5.73 | 107.34 | 40.65 | 54.86 |
| 27 | 20 | 33.3 | 3000 | 1000 | 0 | 1 | 338 | 388.4 | 6.48 | 90.96 | 34.49 | 75.14 |
| 28 | 20 | 20 | 1750 | 3500 | 700 | 0.2 | 165 | 288.5 | 16.28 | 43.48 | 13.14 | 8.53 |
| 29 | 6 | 60 | 500 | 1000 | 700 | 1 | 410 | 430.6 | 5.48 | 256.52 | 68.86 | - 63.47 |
| 30 | 6 | 20 | 2166 | 1000 | 0 | 1 | 202 | 302.4 | 8.02 | 14.12 | 4.71 | 116.75 |
| 31 | 15.3 | 60 | 3000 | 2666 | 0 | 0.2 | 428 | 448.4 | 5.78 | 141.8 | 55.26 | 56.22 |
| 32 | 20 | 60 | 3000 | 3500 | 700 | 0.47 | 409 | 436.5 | 5.59 | 255.65 | 71.18 | - 62.73 |
| 33 | 6 | 60 | 3000 | 1000 | 0 | 0.73 | 424 | 448.2 | 5.67 | 139.55 | 55.19 | 53.24 |
| 34 | 6 | 20 | 3000 | 2250 | 700 | 1 | 161 | 292.2 | 16.62 | 40 | 14.59 | 10.80 |
| 35 | 20 | 20 | 3000 | 3500 | 0 | 0.2 | 198 | 293.4 | 6.93 | 11.86 | 1.59 | 87.29 |
| 36 | 6 | 20 | 500 | 1833 | 700 | 0.2 | 164 | 296.3 | 14.82 | 42.61 | 16.19 | - 1.20 |
| 37 | 6 | 20 | 500 | 3500 | 700 | 0.73 | 169 | 294.8 | 16.04 | 46.96 | 15.61 | 6.93 |
| 38 | 10.6 | 46.7 | 3000 | 1000 | 700 | 0.2 | 358 | 403.8 | 8.37 | 211.30 | 58.35 | - 44.2 |

20 deg). However, when the deformation angle is high, the ductility drops slightly followed by a gentle rise as the temperature increases from 0 °C to 700 °C.

The parameters conducive for promoting the strength include intermediate values of rotation and step size, low annealing temperature, high tool diameter, and low feed rate. These conditions contradict those found favorable for improving the ductility.

C. Microstructure and Tensile Properties

Figures 5(a) through (e) shows the representative grain structures of the unformed and formed (against high and low levels of strength and applied strain) clad sheet. As observed in Figures 5(c) through (e), the grains after ISF become elongated and aligned in the sheet stretching direction. When comparing the pre- and post-ISF microstructures, it can be seen that ISF processing led to grain refinement and the formation of the lamellar structure. In the entire range of investigation, the

average size of post-ISF grains (η in terms of width) varies from 5.78 to 8.11 μm in comparison to the parent grains of 13 μm . It is also evidenced from Figures 5(c) through (e) that there is no grain boundary sliding even for the high strain (*e.g.*, 0.8, in test 14), which means that the ISF process resulted only in the reorientation and refinement of grains.

Figure 6 presents correlations between the grain size and post-ISF strength. There are increases in the yield strength and tensile strength, respectively, from 161 to 430 and 288 to 449 MPa, as the grain size decreases from 8.11 to 5.78 μm . This finding may be attributed to the corresponding increase in the misorientation angle and dislocation density with a decrease in grain size.^[23] The post-ISF yield strength and tensile strength as a function of grain size can be expressed as follows:

$$\sigma_y = -823 + 3059/\sqrt{\eta} \quad [3]$$

$$\sigma_t = -342 + 1931/\sqrt{\eta} \quad [4]$$

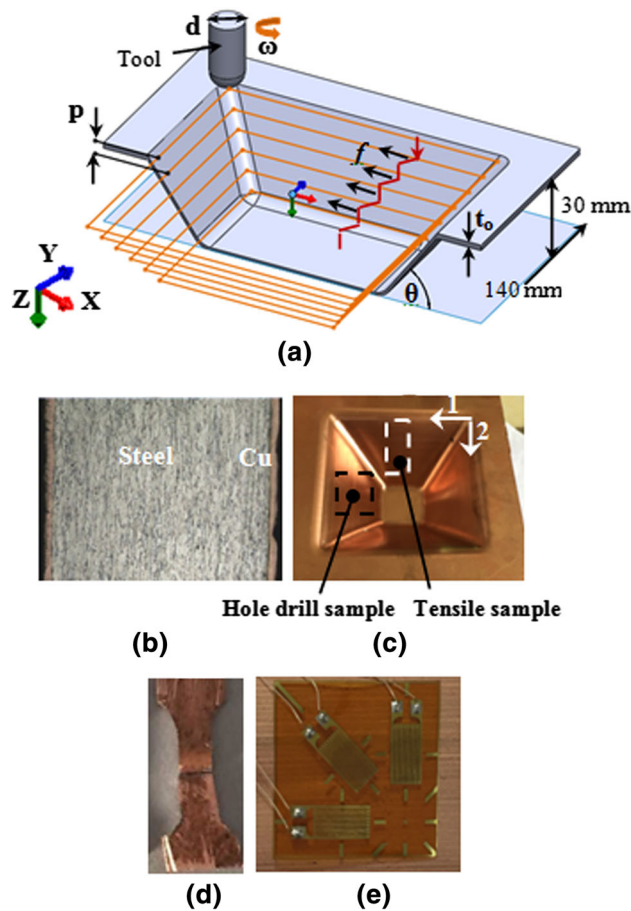


Fig. 1—Experimental methodology: (a) schematic of ISF process, (b) Cu/Steel/Cu clad sheet, (c) formed pyramid, (d) representative tensile sample, and (e) strain rosette attached to formed sheet for hole drill test.

where σ_y is the post-ISF yield strength, σ_t is the post-ISF tensile strength, and η is the average grain width in the cross section.

The preceding equations represent a form of Hall–Petch relation with a negative value of σ_o (friction stress). Hansen reported that the Hall–Petch relation acquires a steep slope with a negative value of σ_o when a material is subjected to a large strain in a forming process.^[23] The strain in the present study was applied up to a high value of 71 pct and the slope of the Hall–Petch relation was also sharp (Figure 6), which justifies the occurrence of native σ_o in Eqs. [3] and [4]. The Hall–Petch correlations were based on only the Steel grains; the Cu grains were not counted because the thickness of the Cu layer was rather small (*i.e.*, 0.05 mm on starting, which further reduced to 0.025 mm on forming) to have any significant influence on the strength. Moreover, the presented relations are free from the adverse effects of grain boundary sliding because such a mechanism did not operate during ISF, as observed from the optical micrographs shown in Figures 5(c) through (e).

Because of the frictional heating during ISF,^[24] there is a possibility of the formation of new compounds/

phases in the clad sheet. In order to identify if any new phase was developed during ISF, selected samples processed with high heat input conditions (*i.e.*, high rotation, low feed, and small step size) were subjected to XRD and EDS tests. For comparison, these tests were also performed on the unformed sheet. The XRD test was conducted on the Cu surface that remained intact with the forming tool during forming, while the EDS was conducted on the Cu/Steel interface. Figure 7 and Table IV present the results of these tests. Figure 7 shows only Cu peaks, which confirms that no new phase was formed during ISF. From Table IV, the formation of a Fe-Cu intermetallic can be observed at the interface of the annealed Cu/Steel sheet (serial numbers 2, 4, and 5). However, its width remains unchanged (*i.e.*, $< 5 \mu\text{m}$) upon ISF, which confirms that the intermetallic occurred only due to annealing.

D. Applied Plastic Strain, Residual Stress, and Tensile Properties

Figure 8 presents the post-ISF tensile properties as a function of applied plastic strain (*i.e.*, strain applied on the sheet during ISF and denoted as ε_{ISF}). The yield strength increases from 161 to 430 MPa, the tensile strength increases from 288 to 449 MPa, and the ductility decreases from 16.62 to 4.93 pct as the applied strain increases from 0.08 to 0.8. In order to elucidate their role on the tensile properties, the effects of the grain size η and mean residual stress σ_m (*i.e.*, mean of σ_2) are superimposed. As is observed, the grain size decreases from 8.11 to 5.78 μm and the residual stress increases from -15 to -131 MPa with increasing applied strain from 0.08 to 0.8. These results imply that the strain-induced variations in the post-ISF tensile properties occur due to the corresponding variations in the grain size and mean residual stress. Further, the tensile properties, applied strain, grain size, and residual stress are correlated. The trend for the residual stress being inversely related to the grain size in the ISF process also follows that reported for traditional forming processes.^[11]

Figure 8 also shows that the yield strength approaches the tensile strength as the applied strain increases. This is due to the fact that the strain hardening rate decreases when a prestrained material (*e.g.*, ISF sheet) is subjected to further deformation (*e.g.*, uniaxial stretching), a condition associated with the saturation of the dislocation density.^[11]

As discussed, the tensile properties are influenced by various factors such as grain size, residual stress, and applied strain. Figures 2 through 4 show that the tensile properties also depend upon the technological parameters. This demonstrates that there is a correlation among the said quantities, tensile properties, and parameters. This is exemplified through the stress–tensile strength relation. The post-ISF tensile strength increases from 403 to 438 MPa due to an increase in the residual stress from -38 to -58 MPa as the condition of the sheet blank in test 38 is changed from annealed (*i.e.*, 700 °C) to rolled (*i.e.*, 0 °C). The tensile strength once again increases from 403 to 430 MPa when the

Table III. ANOVA for Various Responses with the Quadratic Fit Model

| Source | σ_y | | | σ_t | | | λ | | |
|----------------|-----------------------|----------|-------------|-----------------------|----------|-------------|-----------|----------|-------------|
| | F-value | P-value | Significant | F-value | P-value | Significant | F-value | P-value | Significant |
| Model | 590 | < 0.0001 | Y | 279.44 | < 0.0001 | Y | 53.13 | < 0.0001 | Y |
| d | 7.98 | 0.018 | Y | 3.9 | 0.0765 | N | 4.79 | 0.05 | Y |
| θ | 10.716 | < 0.0001 | Y | 5158 | < 0.0001 | Y | 402 | < 0.0001 | Y |
| ω | 0.17 | 0.6928 | N | 1.03 | 0.3343 | N | 0.077 | 0.7867 | N |
| f | 5.39 | 0.0427 | Y | 2.32 | 0.1587 | N | 3.98 | 0.0741 | N |
| T | 149 | < 0.0001 | Y | 15 | 0.0031 | Y | 274 | < 0.0001 | Y |
| p | 0.034 | 0.8575 | N | 0.22 | 0.6455 | N | 3.44 | 0.0933 | N |
| $d\theta$ | 1.76 | 0.2145 | N | 0.04 | 0.8466 | N | 1.43 | 0.2599 | N |
| $d\omega$ | 1.45 | 0.2558 | N | 0.49 | 0.5011 | N | 1.74 | 0.2163 | N |
| df | 1.34 | 0.2746 | N | 0.42 | 0.5311 | N | 6.98 | 0.0247 | Y |
| dT | 15 | 0.0033 | Y | 4.23 | 0.0667 | N | 0.48 | 0.505 | N |
| dp | 24 | 0.0006 | Y | 12.37 | 0.0056 | Y | 18.01 | 0.0017 | Y |
| $\theta\omega$ | 2.18 | 0.1703 | N | 1.56 | 0.2407 | N | 1.62 | 0.2322 | N |
| θf | 2.64 | 0.1353 | N | 0.94 | 0.3558 | N | 0.52 | 0.4869 | N |
| θT | 43.9 | < 0.0001 | Y | 1.36 | 0.27 | N | 313 | < 0.0001 | Y |
| θP | 4.48 | 0.0604 | N | 0.63 | 0.4466 | N | 1.73 | 0.2182 | N |
| ωf | 0.24 | 0.6334 | N | 1.35×10^{-3} | 0.9714 | N | 0.75 | 0.4055 | N |
| ωT | 5.05 | 0.0484 | Y | 5.93 | 0.0352 | Y | 1.5 | 0.2487 | N |
| ωp | 0.84 | 0.3821 | N | 1.44 | 0.2573 | N | 0.16 | 0.7002 | N |
| fT | 4.93 | 0.05 | Y | 8.14 | 0.0172 | Y | 0.55 | 0.4738 | N |
| fp | 3 | 0.114 | N | 0.48 | 0.5027 | N | 1.1 | 0.3196 | N |
| Tp | 0.025 | 0.8785 | N | 0.04 | 0.8394 | N | 1.46 | 0.2548 | N |
| d^2 | 3.61×10^{-3} | 0.9533 | N | 0.3 | 0.595 | N | 0.7 | 0.4239 | N |
| θ^2 | 109.27 | < 0.0001 | Y | 57.93 | < 0.0001 | Y | 1.75 | 0.2156 | N |
| ω^2 | 12.46 | 0.0055 | Y | 2.85 | 0.1223 | N | 0.68 | 0.4281 | N |
| f^2 | 4.28 | 0.0653 | N | 1.15 | 0.3096 | N | 1.08 | 0.3232 | N |
| T^2 | 2.1 | 0.1775 | N | 0.11 | 0.752 | N | 9.6 | 0.0113 | Y |
| p^2 | 8.72 | 0.0145 | Y | 3.85 | 0.0782 | N | 2.81 | 0.1248 | N |

deformation angle in test 38 is varied from 46 to 60 deg, causing a respective change in the residual stress from - 38 to - 87 MPa. The increase in the feed rate from 1000 to 3500 mm/min in test 38 leads to a respective increase in the residual stress from - 38 to - 42 MPa as well as in the tensile strength from 403 to 409 MPa. These results confirm that the variations presented in Figure 8 are caused by the parameters; hence, the post-ISF properties, process parameters, and quantities, such as residual stress, strain, and grain size, are correlated.

IV. DISCUSSION

Figures 9(a) and (b) present a number of stress-strain curves of the Cu/Steel clad sheet. The post-ISF sheet, contrary to the pre-ISF sheet, irrespective of the state of the starting blank, experiences local necking when subjected to uniaxial tension (Figure 9(a)). It follows that the ISF process probably induces inhomogeneities (e.g., variations in the thickness, microstructure, or micropores) in the sheet material. Despite such defects, if any, ISF raises the strength of the sheet. From Figure 9(a), it can be seen that a gain in the ductility can also be realized besides a gain in the strength (Table II provides detailed results). Thus, one can enhance the toughness of the material through the ISF process. Figure 9(b) compares the true stress-strain plots for the

pre- and post-ISF sheets. The plots reveal that the pre-ISF sheet in comparison to the post-ISF sheet hardens at a greater rate. Moreover, the hardening rate during the tension test further drops as the pretension strain imposed on the sheet during ISF increases from 0.08 in test 2 to 0.8 in test 21. This fact is further endorsed by the strain hardening exponent that drops from 0.09 to 0.015 as the ISF strain increases from 0.08 to 0.8, whereas the exponent value for the pre-ISF sheet (shown in Figure 9(b)) is 0.15. The said drop found in the hardening rate can be associated with the attainment of saturation in the dislocation density^[1] and further explains the earlier finding that the post-ISF yield strength approaches the post-ISF tensile strength as the applied ISF strain increases.

The changes (i.e., increase/decrease with reference to the starting unformed blank) in the tensile properties, which the sheet experienced upon ISF, are plotted against the applied strain ϵ_{ISF} in Figure 10. It can be seen that the sheet upon ISF experiences significant gains in both the yield strength and tensile strength (i.e., pct σ_y and pct σ_t , respectively) for any given value of strain. Further, the degree of these gains increases with applied strain. Moreover, for any given value of applied strain, a rise in the yield strength is greater than that in the tensile strength, which can be attributed to a saturation in the dislocation density, as explained earlier. For the strain ranging from 0.08 to 0.8, the rise

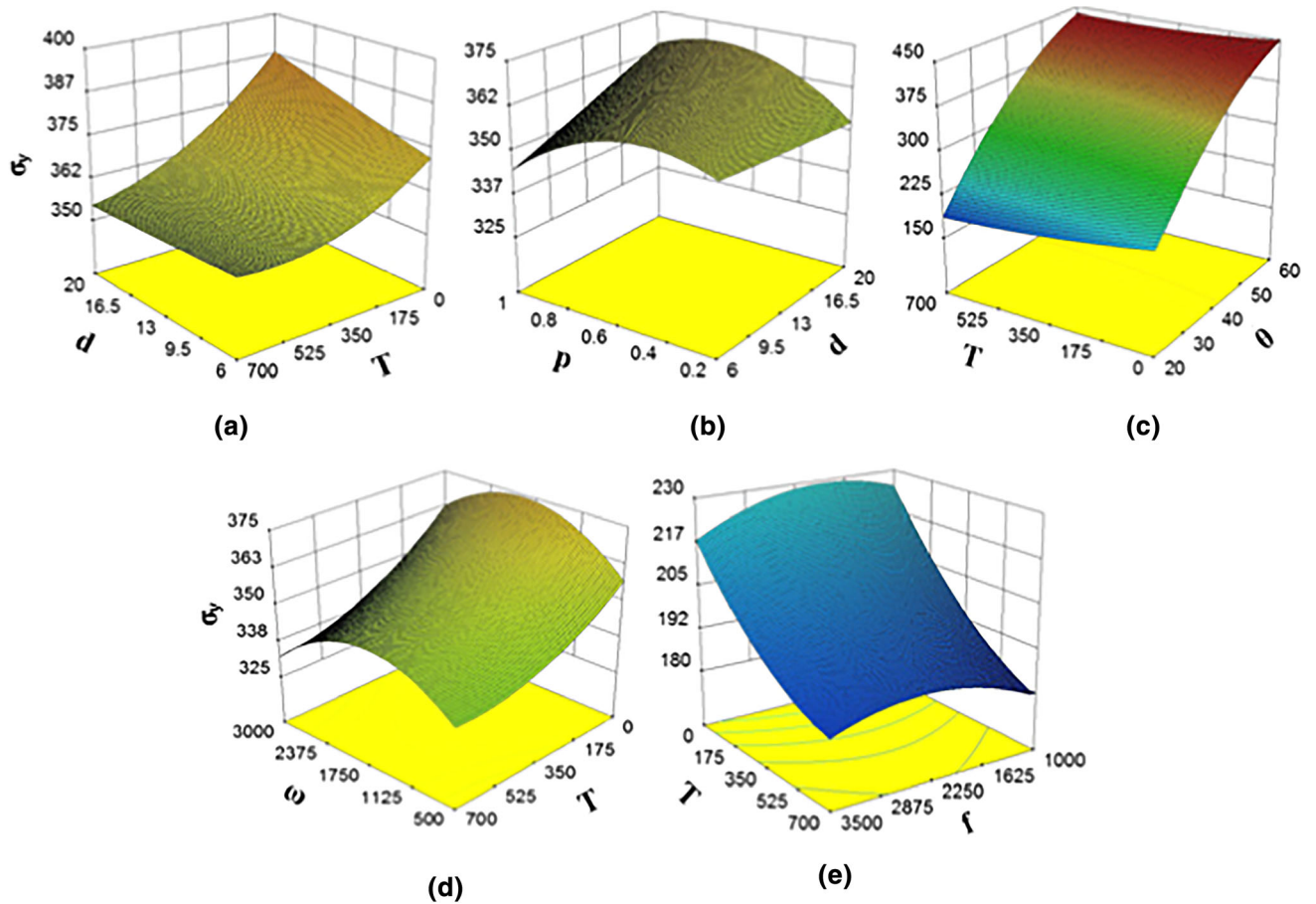


Fig. 2—Effects of parameters on yield strength: (a) diameter and temperature, (b) step size and diameter, (c) temperature and deformation angle, (d) rotation and temperature, and (e) temperature and feed rate.

in the yield strength correspondingly ranges from 10 to 256 pct and that in the tensile strength ranges from 0.6 to 73 pct. The in-depth analysis of Figure 10 reveals that the data points located above a fit curve are associated with the annealed blank, while those located below the curve are associated with the rolled (or annealed at a low temperature) blank. This finding demonstrates that an annealed blank experiences a greater increase in strength upon forming compared with a rolled blank. For instance, the yield strength of the annealed blank increases 253 pct for an applied strain of 0.8 compared with a rolled blank whose yield strength increases 140 pct for an equivalent applied strain. This substantial difference dictates that the annealed blank during ISF encountered a greater hardening rate than the rolled one during ISF.

Contrary to pct σ_y and pct σ_t , pct λ (change in ductility upon ISF) does not establish any consistent relation with the applied ISF strain. However, an important and interesting fact was that the Cu/Steel clad sheet generally showed an increase in ductility (or elongation) upon ISF along with an increase in strength. Overall, the gain in the ductility ranged from 4.6 to 117 pct. The ductility decreased from -1.2 to -67 pct in those instances when the ductility dropped upon ISF. In fact, as revealed by the data in Table II, the nature of

the effect of the ISF process on post-ISF ductility is primarily linked with the forming conditions, specifically the state of the blank sheet and applied strain (*i.e.*, deformation angle). The ductility of the sheet upon ISF increases, regardless of the value of ISF strain, if the starting blank is rolled, as indicated in the figure. However, the gain is greater when low strains are applied while ISF (*e.g.*, < 0.4 or $\theta < 45$ deg). The annealed blank can also show an increase in ductility when the applied strain is low. However, an annealed blank always experiences a drop in ductility if high strains are applied (*e.g.*, > 0.4), as indicated with the dotted rectangles in Figure 10.

Summarizing the results plotted in Figure 10, the prestrained (*i.e.*, rolled) Cu/Steel clad sheet blank upon ISF experiences substantial gains in both strength (yield/tensile) and ductility. The annealed sheet blank, however, observes such a scenario only if the strain value is low (*e.g.*, < 0.4) but shows a drop in ductility if the strains are high (*e.g.*, > 0.4). Moreover, despite experiencing the same forming conditions, an annealed blank in comparison to a rolled blank attains a greater strength increase.

The past studies have identified three competing mechanisms that operate during ISF depending on the forming conditions. These include thermal softening due

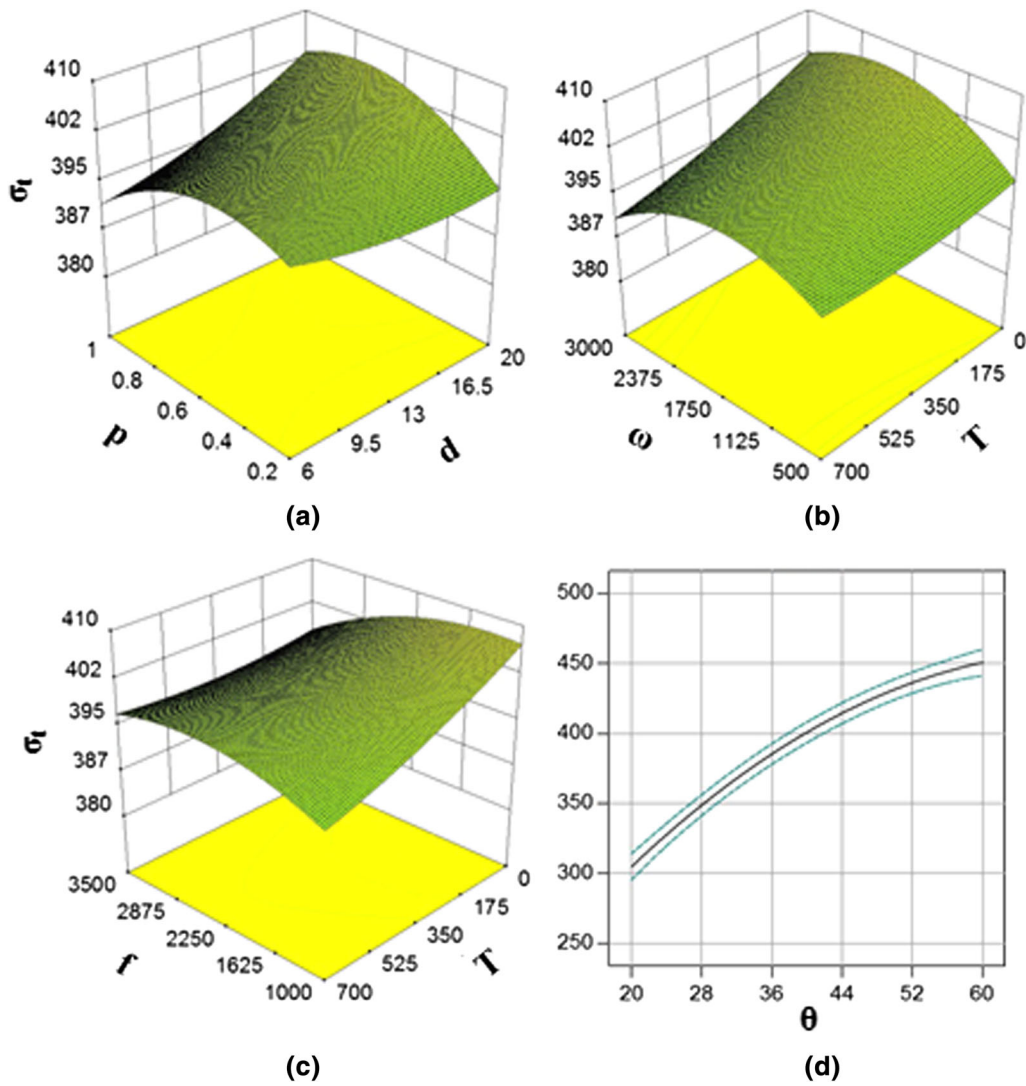


Fig. 3—Effects of parameters on tensile strength: (a) step size and diameter, (b) rotation and temperature, (c) feed rate and temperature, and (d) deformation angle.

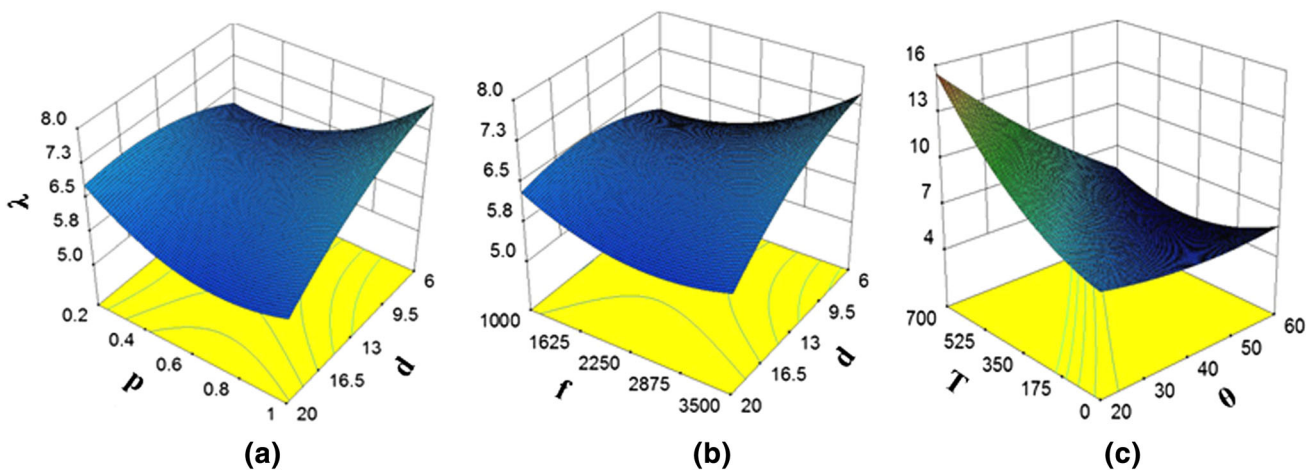


Fig. 4—Effects of parameters on ductility: (a) step size and diameter, (b) feed rate and diameter, and (c) annealing temperature and deformation angle.

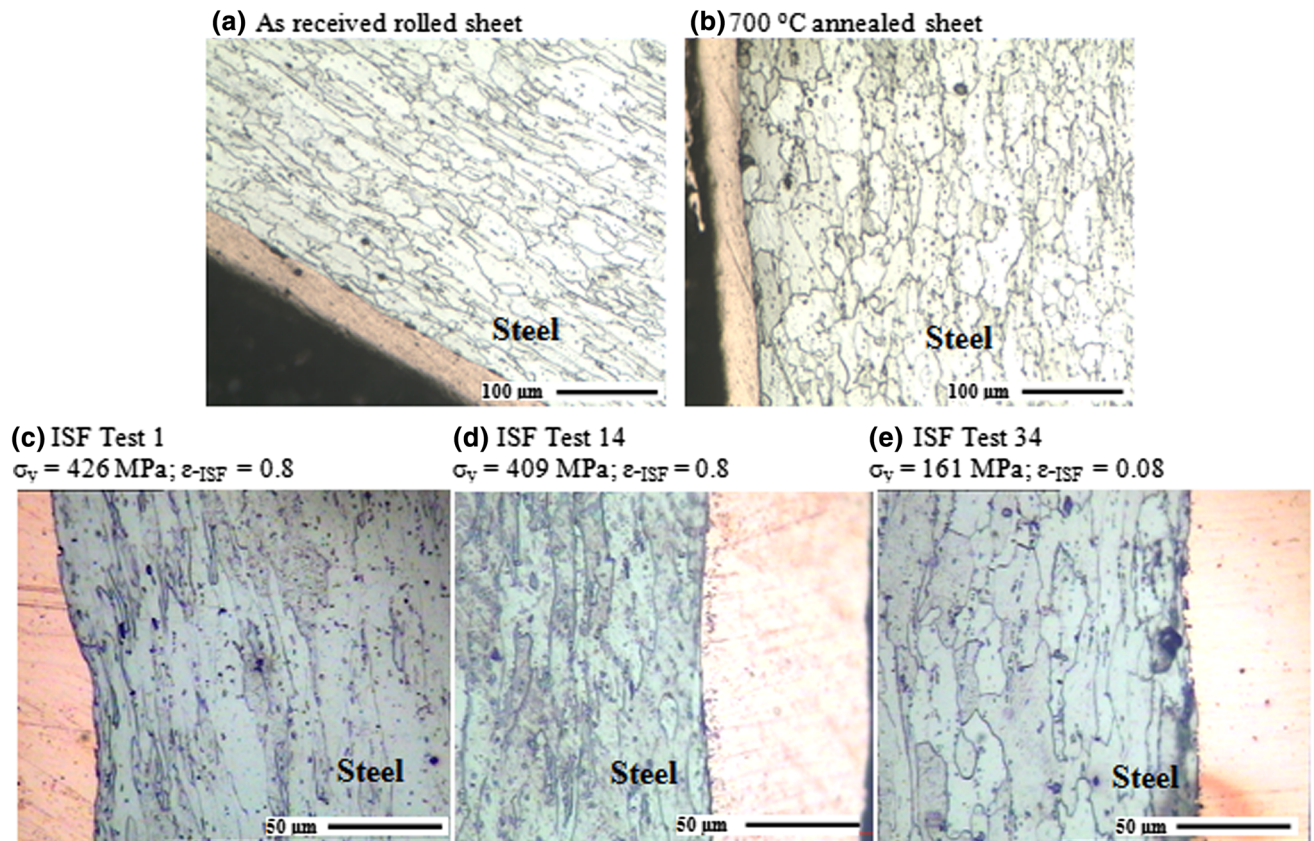


Fig. 5—Optical micrographs of Cu/Steel/Cu clad sheet: (a) as-received rolled sheet, (b) sheet annealed at 700 °C, (c) ISF test 1, (d) ISF test 14, and (e) ISF test 34.

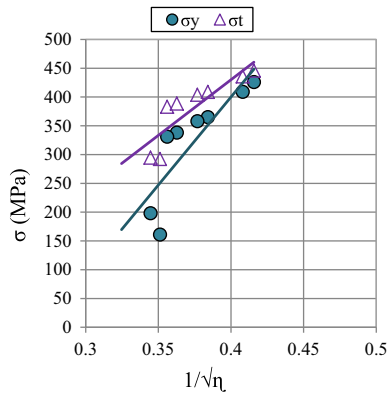


Fig. 6—Relationship between grain size and post-ISF strength.

to frictional heating and straining,^[24,25] dynamic recrystallization due to the stirring action of the forming tool,^[26,27] and strain hardening due to stretching of the sheet.^[18] Thermal softening tends to impart ductility at the cost of strength, dynamic recrystallization (when this occurs) refines grains and enhances both ductility and strength, and strain hardening enhances the strength at the cost of ductility of the material. The tests in which both the ductility and strength increased upon ISF indicate that dynamic recrystallization was dominant over the other two mechanisms, while those where strength increased at the cost of ductility signify

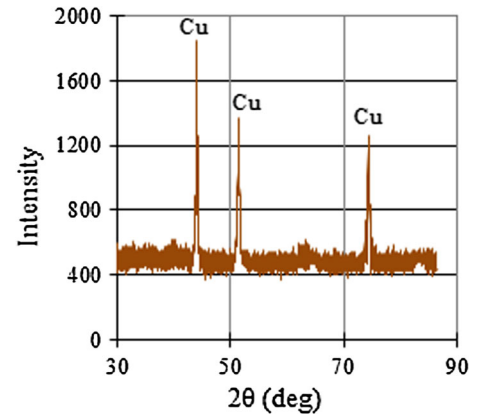
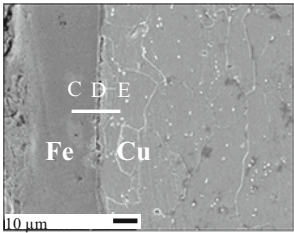
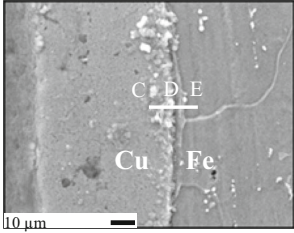
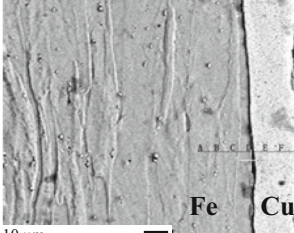
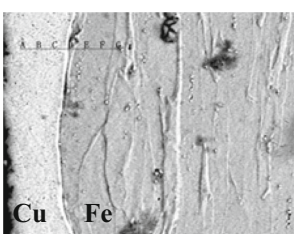
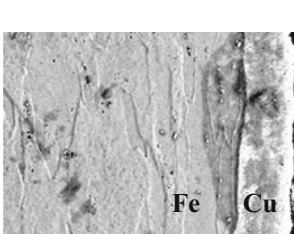


Fig. 7—XRD analysis of post-ISF Cu/Steel/Cu clad sheet with Cu exposed to X-rays.

domination of strain hardening. A prestrained material (*i.e.*, rolled sheet in this case) may undergo recovery^[1] and dynamic recrystallization upon mechanical stirring at low temperatures due to the high strain energy imparted to the sheet. Therefore, a rolled sheet (in comparison to an annealed sheet) exhibits a higher gain in ductility upon being processed by ISF. Further, a decrease in the ductility gained with increasing ISF strain, especially in the rolled blank, indicates gradual domination of strain hardening over dynamic

Table IV. EDS Composition at the Cu/Steel Interface: Pre- and Post-ISF Results

| No. | SEM Image | Composition | | | ISF Conditions | | | | | | Remark |
|-----|---|------------------------------|------------------------|----------------|----------------|----------|----------|----------|----------|----------|----------|
| | | Pct Cu | Pct Fe | Intermetallic | <i>d</i> | θ | ω | <i>f</i> | <i>T</i> | <i>p</i> | |
| 1 |  | C 3.8 D 7.2 E 95 | 96.2 92.8 5 | — — — | — | — | — | — | 400 | — | unformed |
| 2 |  | C 93.7 D 79.64 E 8.99 | 6.3 20.36 91.01 | — CuFe — | — | — | — | — | 700 | — | formed |
| 3 |  | C 4.59 D 6.72 E 95.13 | 95.41 93.28 4.87 | — — — | 20 | 60 | 3000 | 1000 | 400 | 0.2 | formed |
| 4 |  | C 93.28 D 25.45 E 4.32 | 6.72 74.55 95.68 | — CuFe — | 20 | 60 | 3000 | 1000 | 700 | 0.2 | formed |
| 5 |  | C 1.68 D 28.7 E 98.32 | 94.17 71.4 5.83 | — CuFe — | 6 | 60 | 3000 | 1000 | 700 | 0.2 | formed |

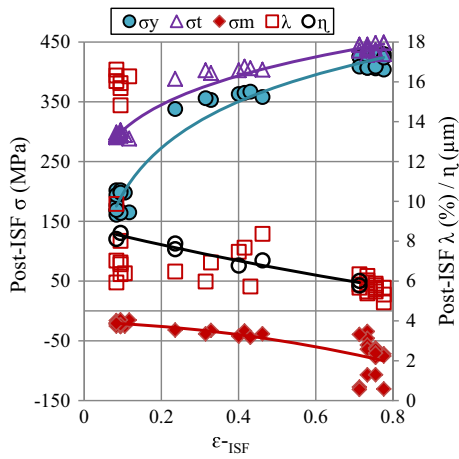


Fig. 8—Tensile properties, residual stress, and grain size as a function of applied plastic strain.

recrystallization and thermal softening. However, exact temperature measurements using an infrared camera and various microstructural analyses (*e.g.*, electron backscatter diffraction (EBSD)) are required to further uncover the underlying facts.

In addition to the state of the material and the strain value (or deformation angle), the other parameters, such as tool diameter, step size and spindle rotation, and feed rate, also affect the strength of material, as detailed before and shown in Figures 2 through 4. These parameters have influence on stirring and heating and, thus, can affect the temperature and activation of the aforementioned mechanisms.^[25] For instance, the greater values of diameter and step size can elevate the temperature and, thus, may promote thermal softening. The higher values of speed may activate mechanical recrystallization along with a rise in temperature. Finally, an increased feed rate can increase the strain

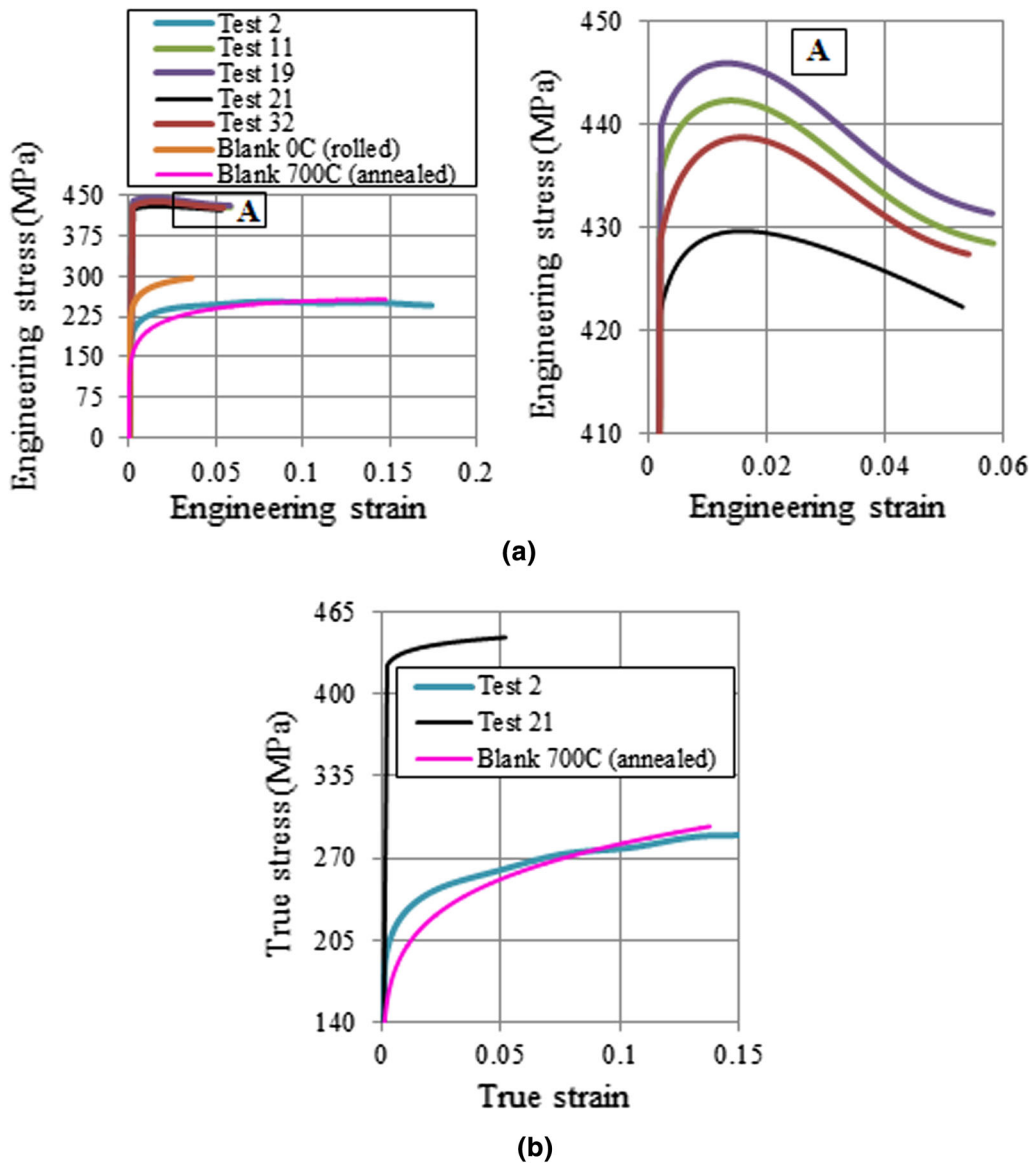


Fig. 9—Stress-strain plots for pre-ISF and post-ISF Cu/Steel/Cu clad sheet: (a) engineering stress-strain curves and (b) true stress-strain curves.

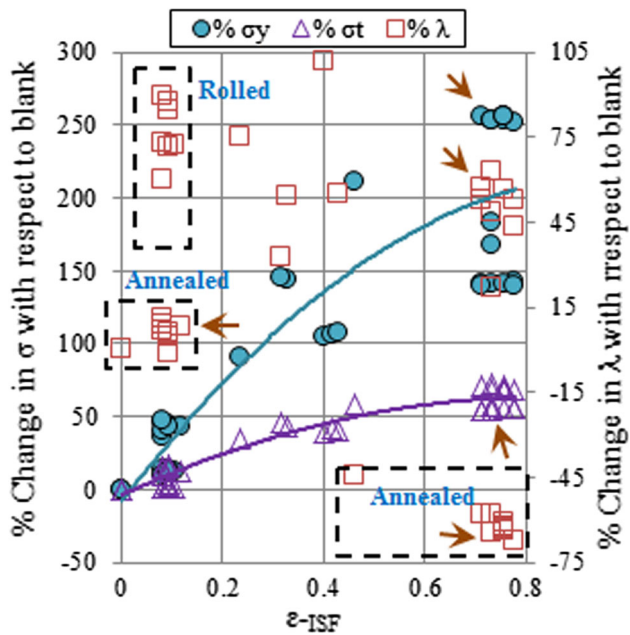


Fig. 10—Post-ISF tensile properties with respect to starting blank.

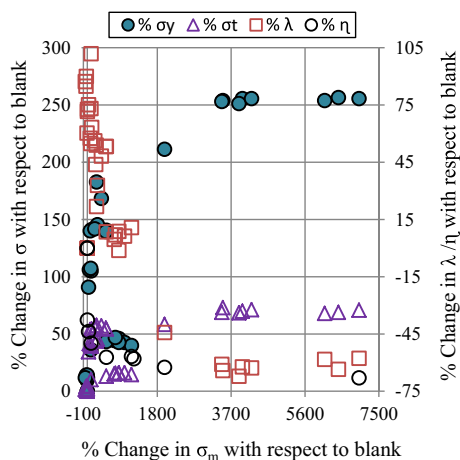


Fig. 11—Correlation between percent change in residual stress and tensile properties.

rate and temperature.^[25] The effects of these parameters on the tensile properties of the present material are highlighted with rectangles in Figure 10. These parameters are, however, less significant compared with the applied strain and state of material.

Figure 11 plots the percent tensile properties as a function of the percent value of residual stress. There is an increase in pct σ_y and pct σ_t and a decrease in pct λ with an increase in pct σ_m (pct λ turns negative when pct σ_m is very high, *e.g.*, > 1000 pct). A similar trend can be seen against percent change in the grain size (*i.e.*, pct η). These findings reveal that pct σ_m , which is correlated to pct η , has a controlling influence on the degree of change in the post-ISF tensile properties of the Cu/Steel clad

sheet. As observed in Figure 11, the material upon ISF experiences a huge variation in residual stress, ranging from -50 to about 7000 pct. Furthermore, the material gains stress in most of the cases. However, a drop in the stress value also occurs in a few tests (*i.e.*, 6, 9, 18, and 35) wherein the applied strain was low and the material had a rolled state. This stress drop, which probably happened due to dynamic recrystallization, further explains the reason for the aforementioned gains in ductility.

The results reported in this study demonstrate that the ISF process can produce components with greatly enhanced properties and, thus, has the potential to enable lightweight design and cost savings. The results detailed in this study are, however, valid for the widely observed plane-strain deformation, although, depending on the shape and size of a component, the sheet in ISF may experience different strain paths (*e.g.*, plane strain on the flat surface and biaxial strain on the corners in a pyramid^[13]). Since the degree of strain hardening in a metal forming process depends upon the strain path,^[28] mechanical properties as a function of strain path should be investigated in the future in order to deepen understanding and widen the process applications.

V. CONCLUSIONS

The influence of ISF processing on the mechanical properties of the Cu-clad Steel sheet was investigated in this study. The important findings of the study are as follows.

1. The ISF process substantially affected the tensile properties of the clad sheet. Depending on the forming conditions, the post-ISF values of yield strength, tensile strength, and ductility ranged from 161 to 430, 288 to 449 MPa, and 4.93 to 16.62 pct, respectively. The deformation angle and initial state of the material (annealing temperature) were found to be the most significant parameters on the properties obtained following ISF.
2. The sheet experienced substantial gains following the ISF process in the various properties: yield strength (4.6 to 117 pct) and tensile strength (0.6 to 73 pct). The gain in ductility occurred when the process was performed on the prestrained blank (*i.e.*, rolled) but dropped when large forming strains (*e.g.*, < 0.4) were applied on the annealed blank. The ductility ranged from -67 to 117 pct.
3. The grain size decreased from 8.11 to 5.78 μm with an increase in plastic strain from 0.08 to 0.8, while the mean residual stress increased from -15 to -131 MPa. The post-ISF yield and tensile strengths increased, while the post-ISF ductility of the sheet decreased. The tensile properties, applied strain, grain size, and residual stress are thus correlated. The post-ISF strength was also shown to obey the Hall-Petch relationship.

4. EDS and XRD analyses confirmed that no new phase formed due to ISF processing.

VI. FUTURE WORK

EBSD analysis will be conducted in the future to add knowledge on the deformation mechanism(s) that operated during ISF of the Cu/Steel clad sheet. The mechanism of dynamic recrystallization will also be explored, in particular, the relation to the initial state of the blank material. Work will also be conducted to understand the effect of the strain path on strain hardening upon ISF in order to widen the application window. Another important future task is to develop a generic model in order to predict the post-ISF mechanical properties of various materials.

ACKNOWLEDGMENTS

The authors are thankful of GIK Institute of Engineering Sciences & Technology, Pakistan, for providing necessary technical support to materialize this research.

FUNDING

This research work was supported by the Fundamental Research Funds for the Central Universities, People's Republic of China (Grant No. NS2015055), National Natural Science Foundation of China (Grant No. 51105202); and the State Administration of Foreign Experts Affairs, People's Republic of China, and the Ministry of Education, People's Republic of China (111 Project—Grant No. 773 B16024).

NOMENCLATURE

| | |
|--------------------|----------------------------------|
| d | Tool diameter |
| θ | Deformation angle |
| ω | Tool rotation |
| f | Feed rate |
| p | Step size |
| T | Annealing temperature |
| σ_t | Post-ISF tensile strength |
| σ_y | Post-ISF yield strength |
| λ | Ductility or percent elongation |
| η | Grain width in the cross section |
| ISF | Incremental sheet forming |
| ε -ISF | Strain applied by ISF |
| EDS | Electron dispersive spectroscopy |
| XRD | X-ray diffraction |
| SEM | Scanning electron microscope |
| EBSD | electron backscatter diffraction |

REFERENCES

1. W.F. Hosford and R.M. Caddell: *Metal Forming Mechanics and Metallurgy*, 4th ed., Cambridge University Press, New York, NY, 2011, pp. 237–53.
2. G. Hussain, L. Gao, N. Hayat, and X. Ziran: *J. Mater. Process. Technol.*, 2009, vol. 209, pp. 4237–42.
3. Y. Mu, B. Wang, J. Zhou, X. Huang, and X. Li: *Metall. Mater. Trans. A*, 2017, vol. 48A, pp. 2017–5467.
4. S. Serajzadeh and M. Mohammadzadeh: *Int. J. Adv. Manuf. Technol.*, 2007, vol. 34, pp. 262–69.
5. Y. Zhao, B. Song, J. Pei, C. Jia, B. Li, and G. Linlin: *J. Mater. Process. Technol.*, 2013, vol. 213, pp. 1855–63.
6. S.A. Balogun, D. Esezobor, and S.O. Adeosun: *Metall. Mater. Trans. A*, 2007, vol. 38A, pp. 1570–74.
7. Y. Mo, Y. Jiang, X. Liu, and J. Xie: *Mater. Sci. Eng. A*, 2016, vol. 670, pp. 122–31.
8. S. Sepahi-Boroujeni and A. Sepahi-Boroujeni: *J. Manuf. Process.*, 2016, vol. 24, pp. 71–77.
9. J. Xu, D. Shan, X. Wang, B. Guo, M. Shirooyeh, T.G. Langdon, and G. Xing: *J. Mater. Sci.*, 2015, vol. 50, pp. 7424–36.
10. R.B. Figueiredo and T.G. Langdon: *J. Mater. Sci.*, 2010, vol. 45, pp. 4827–36.
11. F.O. Neves, D.U. Braga, and A.S.C. Silva: *Mater. Manuf. Process.*, 2015, vol. 30, pp. 1278–82.
12. S.B.M. Echrif and M. Hrairi: *Mater. Manuf. Process.*, 2011, vol. 26, pp. 1404–14.
13. M.B. Silva, M. Skjoedt, P.A.F. Martins, and N. Bay: *Int. J. Mach. Tool. Manuf.*, 2008, vol. 48, pp. 73–83.
14. K.A. Al-Ghamdi and G. Hussain: *Int. J. Mach. Tool. Manuf.*, 2015, vol. 88, pp. 82–94.
15. L. Van-Sy and N.T. Nam: *J. Manuf. Technol. Res.*, 2014, vol. 6, pp. 17–31.
16. J. Park, J. Kim, N. Park, and Y. Kim: *Metall. Mater. Trans. A*, 2010, vol. 41A, pp. 97–105.
17. G. Hirt, J. Ames, M. Bambach, and R. Kopp: *CIRP Ann.*, 2004, vol. 53, pp. 203–06.
18. J. Jeswiet, E. Hagan, and A. Szekeres: *Proc. IMechE Part B: J. Eng. Manuf.*, 2002, vol. 261, pp. 1367–71.
19. I. Ulacia, L. Galdos, J.A. Esanola, J.L. Aga, G. Arruebarrena, E.S. De-Argandon, and I. Hurato: *Metall. Mater. Trans. A*, 2014, vol. 45A, pp. 3352–77.
20. L.M. Lozano-Sánchez, A.O. Sustaita, M. Soto, S. Biradar, L. Ge, E. Segura-Cárdenas, J. Diabb, L.E. Elizalde, E.V. Barrera, and A. Elias-Zúñiga: *J. Mater. Process. Technol.*, 2017, vol. 242, pp. 218–27.
21. T. Huang-Chi, H. Chinghua, and H. Chin-Chuan: *Int. J. Adv. Manuf. Technol.*, 2010, vol. 49, pp. 1029–36.
22. M.J. Anderson and P.J. Whitcomb: *RSM Simplified—Optimizing Processes Using Response Surface Methods for Design of Experiments*, 2nd ed., Productivity Press, New York, NY, 2005, pp. 75–90.
23. N. Hansen: *Scripta Mater.*, 2004, vol. 51, pp. 801–06.
24. M. Durante, A. Formisano, A. Langella, F. Memola, and C. Minutolo: *J. Mater. Process. Technol.*, 2009, vol. 209, pp. 4621–26.
25. A. Giuseppina, C. Claudion, F. Luigino, and G. Francesco: *Int. J. Mech. Sci.*, 2016, vols. 108–109, pp. 39–48.
26. D. Xu, W. Wu, R. Malhotra, J. Chen, B. Lu, and J. Cao: *Int. J. Mach. Tool. Manuf.*, 2003, pp. 37–46.
27. G. Buffa, D. Campanella, and L. Fratini: *Int. J. Adv. Manuf. Technol.*, 2013, vol. 66, pp. 1343–51.
28. P.R. Cetlin, E.C.S. Corrêa, and M.T.P. Aguiar: *Metall. Mater. Trans. A*, 2003, vol. 34A, pp. 589–601.
29. N.R. Costa, J. Lourenço, and Z.L. Pereira: *Ch. Intell. Lab. Sys.*, 2011, vol. 107, pp. 234–44.

Publisher's Note Springer Nature remains neutral with regard to jurisdictional claims in published maps and institutional affiliations.